Elasticity of spheres with buckled surfaces

Yingzhen Tian [1], Megan McCarthy [2], Megan King [2,3] and S. G. J. Mochrie [1,4]
[1]*Department of Physics, Yale University, New Haven, Connecticut 06511, USA*
[2]*Department of Cell Biology, Yale School of Medicine, New Haven, Connecticut 06520, USA*
[3]*Department of Molecular, Cellular, and Developmental Biology, Yale University, New Haven, Connecticut 06520, USA*
[4]*Department of Applied Physics, Yale University, New Haven, Connecticut 06511, USA*

(Received 23 November 2022; accepted 27 April 2023; published 26 June 2023)

The buckling instabilities of core-shell systems, comprising an interior elastic sphere, attached to an exterior shell, have been proposed to underlie myriad biological morphologies. To fully discuss such systems, however, it is important to properly understand the elasticity of the spherical core. Here, by exploiting well-known properties of the solid harmonics, we present a simple, direct method for solving the linear elastic problem of spheres and spherical voids with surface deformations, described by a real spherical harmonic. We calculate the corresponding bulk elastic energies, providing closed-form expressions for any values of the spherical harmonic degree (l), Poisson ratio, and shear modulus. We find that the elastic energies are independent of the spherical harmonic index (m). Using these results, we revisit the buckling instability experienced by a core-shell system comprising an elastic sphere, attached within a membrane of fixed area, that occurs when the area of the membrane sufficiently exceeds the area of the unstrained sphere [C. Fogle *et al.*, Phys. Rev. E **88**, 052404 (2013)]. We determine the phase diagram of the core-shell sphere's shape, specifying what value of l is realized as a function of the area mismatch and the core-shell elasticity. We also determine the shape phase diagram for a spherical void bounded by a fixed-area membrane.

DOI: 10.1103/PhysRevE.107.065003

I. INTRODUCTION

There has been longstanding interest in the mechanical instabilities of core-shell systems, comprising an elastic sphere on the inside, surrounded by and attached to an elastic exterior shell. Although idealized, such a model has been proposed to underlie myriad buckled or wrinkled biological morphologies, such as those of fruits and vegetables [1–3], insect eggs [4], pollen grains [5,6], neutrophils and B cells [7–9], mammalian brains [10,11], and growing tumors [12]. In addition to these biological examples, swelling gels often show similar mechanical instabilities [13–16], as do inorganic core-shell systems [17,18].

To fully discuss spherical core-shell systems, it is important to properly understand the elasticity of the spherical core. For an isotropic material with Poisson ratio, ν, in mechanical equilibrium, according to linear elasticity theory, the elastic displacement field, $\mathbf{u}$, must satisfy

$$\nabla(\nabla\cdot\mathbf{u})+(1-2\nu)\nabla^2\mathbf{u}=0, \tag{1}$$

which is the statement that the force density is zero everywhere within the material of the spherical core. Equation (1) plays an analogous role in elasticity theory to that played in electrostatics by Laplace's equation, whose solutions are well known to be the regular and irregular solid harmonics, namely $r^l Y_l^m(\theta,\phi)$ and $r^{-l-1}Y_l^m(\theta,\phi)$, respectively. From this point of view, it is surprising that analytic solutions of Eq. (1) in near spherical situations have been little discussed. The corresponding elastic energies of these solutions also remain unknown, as far as we are aware. Reference [19] sought to remedy this situation by, first, solving Eq. (1) for an elastic sphere subject to the boundary condition that the sphere's surface is displaced radially with an amplitude given by a real spherical harmonic and, then, by calculating the corresponding elastic energies. However, as described below, we disagree with Ref. [19]'s result that the elastic energy depends on the spherical harmonic index, m.

The goal of this paper is threefold: (1) to find the displacement field both within a sphere, with a real-spherical-harmonic surface displacement, and outside a spherical void, with a real-spherical-harmonic surface displacement, (2) to calculate corresponding bulk elastic energies, and (3) to use the resultant elastic energy to determine the shape phase diagram both of a core-shell system, comprising an elastic sphere, attached within a membrane of fixed area [19], and of a spherical void, which is lined by a membrane of fixed area, that is attached to the surrounding elastic medium. A number of recent contributions have focused on postbuckling pattern selection in core-shell systems, which depends on nonlinear effects [3,6,9,10,18,20–23]. However, such phenomena lie beyond our scope, which is confined to linear elasticity only.

The outline of the paper is as follows. By exploiting well-known properties of the solid harmonics, we first present a straightforward, direct method for solving Eq. (1) in general, near-spherical situations, both for spheres (Sec. II) and spherical voids (Sec. III). Then, we fit the general solutions to boundary conditions corresponding to a spherical core (Sec. IV) or a spherical void (Sec. V), whose surface is displaced radially with an amplitude given by a real spherical harmonic. In Sec. VI, we calculate the bulk elastic energies corresponding to these boundary conditions. We provide analytic expressions for the energies for any value of the spherical

harmonic degree, l, Poisson ratio, ν, and shear modulus, μ. The elastic energies are independent of the spherical harmonic index, m. In Sec. VII, following Ref. [19], we revisit the buckling instability experienced by a core-shell system comprising an elastic sphere, attached within a membrane of fixed area, that occurs when the area of the membrane sufficiently exceeds the area of the unstrained sphere. We determine the phase diagram of the core-shell sphere's shape, specifying what value of l is realized as a function of area mismatch and sphere and membrane elasticity. Similarly, we also determine the analogous shape phase diagram for a spherical void bounded by a fixed-area membrane. A MATHEMATICA notebook containing all of our calculations is available as Supplemental Material [24].

II. REGULAR SOLUTION FOR SPHERES

To find solutions to Eq. (1), applicable to (slightly deformed) spheres, we first introduce two trial functions, that when summed together with appropriate relative weighting, indeed satisfy Eq. (1). To this solution, we then add additional terms that each satisfies Eq. (1) on its own, yielding a final result that can be conveniently matched to the applicable boundary conditions.

Trial function 1 takes the form

$$\mathbf{u}_1 = ar^2\nabla\left(r^l Y_l^m\right), \tag{2}$$

where a is a constant. Equation (2) converges at $r = 0$ and eventually will be part of the so-called regular solution. It follows from Eq. (2) that

$$\begin{aligned}\nabla\cdot\mathbf{u}_1 &= a(\nabla r^2)\cdot\nabla\left(r^l Y_l^m\right) + ar^2\nabla^2\left(r^l Y_l^m\right)\\ &= 2lar^l Y_l^m\end{aligned} \tag{3}$$

and, in turn, that

$$\nabla(\nabla\cdot\mathbf{u}_1) = 2la\nabla\left(r^l Y_l^m\right). \tag{4}$$

We also have that

$$\nabla^2\mathbf{u}_1 = 2(2l+1)a\nabla\left(r^l Y_l^m\right). \tag{5}$$

Combining Eqs. (4) and (5) yields

$$\begin{aligned}&\nabla(\nabla\cdot\mathbf{u}_1) + (1-2\nu)\nabla^2\mathbf{u}_1\\ &\quad= [2l + 2(1-2\nu)(2l+1)]a\nabla\left(r^l Y_l^m\right).\end{aligned} \tag{6}$$

Thus Eq. (1) produces a nonzero result for $\mathbf{u}_1$ and another trial function is needed to cancel $\mathbf{u}_1$ in order to satisfy Eq. (1).

To this end, we introduce trial function 2:

$$\mathbf{u}_2 = \mathbf{b}r^{l+1}Y_{l+1}^m, \tag{7}$$

where $\mathbf{b} = (b_x, b_y, b_z)$ is a constant vector. Then,

$$\begin{aligned}\nabla\cdot\mathbf{u}_2 &= \mathbf{b}\cdot\nabla\left(r^{l+1}Y_{l+1}^m\right)\\ &= \alpha r^l Y_l^{m+1} + \beta r^l Y_l^m + \gamma r^l Y_l^{m-1},\end{aligned} \tag{8}$$

where α, β, and γ are all known quantities, given explicitly in Appendix A [Eqs. (A4), (A5), and (A6)]. Since $\nabla^2\mathbf{u}_2 = 0$, we have that

$$\begin{aligned}\nabla(\nabla\cdot\mathbf{u}_2) + (1-2\nu)\nabla^2\mathbf{u}_2 &= \nabla(\nabla\cdot\mathbf{u}_2)\\ &= \alpha\nabla\left(r^l Y_l^{m+1}\right) + \beta\nabla\left(r^l Y_l^m\right)\\ &\quad+ \gamma\nabla\left(r^l Y_l^{m-1}\right).\end{aligned} \tag{9}$$

The terms on the right-hand side of Eq. (9) are of the same form as the right-hand side of Eq. (6), except for the appearance of additional terms with spherical harmonic indices equal to $m \pm 1$. However, we can use a modified version of $\mathbf{u}_1$, augmented to cancel all three terms arising from $\mathbf{u}_2$. Because $\nabla(r^l Y_l^m)$ satisfies Eq. (1) on its own, we can also add additional terms of this form to $\mathbf{u}_1$, with a view to the solution for a surface displacement given by a single spherical harmonic. Specifically, we can pick

$$\begin{aligned}\mathbf{u}_1' &= a_1(r^2 - R^2)\nabla\left(r^l Y_l^{m+1}\right)\\ &\quad+ a_0(r^2 - R^2)\nabla\left(r^l Y_l^m\right)\\ &\quad+ a_{-1}(r^2 - R^2)\nabla\left(r^l Y_l^{m-1}\right),\end{aligned} \tag{10}$$

where R is the radius of the undeformed sphere,

$$a_1 = \frac{-\alpha}{2l + 2(1-2\nu)(2l+1)}, \tag{11}$$

$$a_0 = \frac{-\beta}{2l + 2(1-2\nu)(2l+1)}, \tag{12}$$

and

$$a_{-1} = \frac{-\gamma}{2l + 2(1-2\nu)(2l+1)}. \tag{13}$$

By construction, Eq. (1) is now satisfied by

$$\begin{aligned}\mathbf{u}_{lm} &= \mathbf{u}_1' + \mathbf{u}_2\\ &= a_1(r^2 - R^2)\nabla\left(r^l Y_l^{m+1}\right)\\ &\quad+ a_0(r^2 - R^2)\nabla\left(r^l Y_l^m\right)\\ &\quad+ a_{-1}(r^2 - R^2)\nabla\left(r^l Y_l^{m-1}\right)\\ &\quad+ (b_x, b_y, b_z)r^{l+1}Y_{l+1}^m.\end{aligned} \tag{14}$$

Using the expressions for α, β, and γ, given in the Appendixes, we have

$$a_1 = \frac{(b_x - ib_y)\sqrt{\frac{(2l+3)(l-m+1)!}{(l+m+1)!}}}{2[l(8\nu-6) + 4\nu - 2]\sqrt{\frac{(2l+1)(l-m-1)!}{(l+m+1)!}}}, \tag{15}$$

$$a_0 = \frac{b_z(l+m+1)\sqrt{\frac{(2l+3)(l-m+1)!}{(l+m+1)!}}}{[l(8\nu-6) + 4\nu - 2]\sqrt{\frac{(2l+1)(l-m)!}{(l+m)!}}}, \tag{16}$$

and

$$a_{-1} = -\frac{(b_x + ib_y)(l+m)(l+m+1)\sqrt{\frac{(2l+3)(l-m+1)!}{(l+m+1)!}}}{2[l(8\nu-6) + 4\nu - 2]\sqrt{\frac{(2l+1)(l-m+1)!}{(l+m-1)!}}}. \tag{17}$$

While $\mathbf{u}_1'$ involves spherical harmonics of degree $l-1$, by contrast $\mathbf{u}_2$ involves spherical harmonics of degree $l+1$. Thus solutions to Eq. (1) necessarily involve at least one pair of values of l that differ by 2. We also see that solutions to Eq. (1) naturally involve three consecutive values of m.

For $r = R$, we see that only $\mathbf{u}_2$ survives. Because $\mathbf{u}_2$ involves a single spherical harmonic, this approach facilitates matching surface displacements that are given by a spherical harmonic or a sum of spherical harmonics.

III. IRREGULAR SOLUTION FOR SPHERICAL VOIDS

Using an analogous procedure to that followed in Sec. II, we can also find a solution that remains finite as $r \to \infty$, namely the irregular solution, which is applicable within elastic material surrounding a spherical void. To this end, we again introduce two trial functions,

$$\begin{aligned}\mathbf{v}_1 =& a_1(r^2 - R^2)\nabla\left(r^{-l-1}Y_l^{m+1}\right)\\ &+ a_0(r^2 - R^2)\nabla\left(r^{-l-1}Y_l^{m}\right)\\ &+ a_{-1}(r^2 - R^2)\nabla\left(r^{-l-1}Y_l^{m-1}\right)\end{aligned} \tag{18}$$

and

$$\begin{aligned}\mathbf{v}_2 =& \mathbf{b}r^{-l}Y_{l-1}^m\\ =& (b_x, b_y, b_z)r^{-l}Y_{l-1}^m.\end{aligned} \tag{19}$$

To ensure that $\mathbf{v}_1 + \mathbf{v}_2$ is a solution to Eq. (1), we must pick

$$a_0 = \frac{b_z\sqrt{\frac{-1+2l}{3+2l}}\sqrt{l^2 - m^2}}{2\sqrt{\frac{1+2l}{3+2l}}(-2 - 3l + 2\nu + 4l\nu)}, \tag{20}$$

$$a_1 = -\frac{(b_x - ib_y)\sqrt{\frac{-1+2l}{3+2l}}\sqrt{(l+m)(1+l+m)}}{4\sqrt{\frac{1+2l}{3+2l}}(-2 - 3l + 2\nu + 4l\nu)}, \tag{21}$$

$$a_{-1} = \frac{(b_x + ib_y)\sqrt{\frac{-1+2l}{3+2l}}\sqrt{l + l^2 - 2lm + (-1+m)m}}{4\sqrt{\frac{1+2l}{3+2l}}(-2 - 3l + 2\nu + 4l\nu)}, \tag{22}$$

so that the contributions of the two trial functions to Eq. (1) cancel.

The irregular solution is

$$\begin{aligned}\mathbf{v}_{lm} =& \mathbf{v}_1 + \mathbf{v}_2\\ =& a_1(r^2 - R^2)\nabla\left(r^{-l-1}Y_l^{m+1}\right)\\ &+ a_0(r^2 - R^2)\nabla\left(r^{-l-1}Y_l^{m}\right)\\ &+ a_{-1}(r^2 - R^2)\nabla\left(r^{-l-1}Y_l^{m-1}\right)\\ &+ (b_x, b_y, b_z)r^{-l}Y_{l-1}^m.\end{aligned} \tag{23}$$

Two values of l are involved in the irregular solution too, and only the coefficients in $\mathbf{v}_2$ need be considered to fit boundary conditions at $r = R$.

IV. SPHERE WITH A SPHERICAL HARMONIC SHAPE DEFORMATION

Next, we consider a (slightly deformed) sphere, whose shape deviates from a perfect sphere by a single, real spherical harmonic, Y_{lm}, defined as

$$Y_{lm} = \frac{1}{\sqrt{2}}\left[Y_l^m + (-1)^m Y_l^{-m}\right] \tag{24}$$

for $m > 0$ and as $Y_{l0} = Y_l^0$ for $m = 0$. The amplitude of the displacement of the elastic medium immediately behind the surface is proportional to the surface displacement. We furthermore suppose that this displacement is directed along the radial direction. Thus the relevant boundary condition is that the displacement at the surface is

$$\mathbf{u}(R) = gRY_{lm}\hat{\mathbf{r}}, \tag{25}$$

where g is a dimensionless measure of the amplitude of the surface displacement. The radial unit vector, $\hat{\mathbf{r}} = (\sin\theta\,\cos\phi, \sin\theta\,\sin\phi, \cos\theta)$, may be expressed in terms of Y_1^1, Y_1^0, and Y_1^{-1}:

$$\begin{aligned}\hat{\mathbf{r}} =& \left(-\sqrt{\frac{2\pi}{3}}\left[Y_1^1(\theta,\phi) - Y_1^{-1}(\theta,\phi)\right], i\sqrt{\frac{2\pi}{3}}\left[Y_1^{-1}(\theta,\phi)\right.\right.\\ &\left.\left. + Y_1^1(\theta,\phi)\right], 2\sqrt{\frac{\pi}{3}}Y_1^0(\theta,\phi)\right),\end{aligned} \tag{26}$$

implying that Eq. (25) consists of pairwise products of spherical harmonics. It is well known, however, that pairwise products of spherical harmonics may be expressed as a linear combination of spherical harmonics with degrees and indices and weights, specified by the Wigner 3-j symbols. Thus we find that Eq. (25) contains spherical harmonics with degree $l \pm 1$, and indices $m \pm 1$ for the x and y components, and index m for the z component, and the complex conjugates of these terms, which is a total of twelve spherical harmonics each with a different combination of l and m than the others (Table I). This form of Eq. (25) is given in the accompanying MATHEMATICA notebook. To satisfy these boundary conditions, we must select a solution that is a superposition of twelve $\mathbf{u}_{lm}$'s containing the values of l and m needed, and we must set the components of $\mathbf{b}$ for each $\mathbf{u}_{lm}$ in the superposition equal to the coefficient of the corresponding spherical harmonic in Eq. (25). Thus we find the following solution for spheres:

TABLE I. Spherical harmonics components of shape, displacement, and strain.

	l (sphere)	m (sphere)	l (void)	m (void)
Shape	l	$\pm m$	l	$\pm m$
$u_{x,y}(R)$, $v_{x,y}(R)$	$l \pm 1$	$\pm m \pm 1$	$l \pm 1$	$\pm m \pm 1$
$u_z(R)$, $v_z(R)$	$l \pm 1$	$\pm m$	$l \pm 1$	$\pm m$
$u_{x,y}$, $v_{x,y}$	$l \pm 1$	$\pm m \pm 1$	$l \pm 1$	$\pm m \pm 1$
u_z, v_z	$l \pm 1$	$\pm m$	$l \pm 1$	$\pm m$
$\epsilon_{xx,xy,yx,yy}$	$l, l-2$	$\pm m \pm 2, \pm m$	$l, l+2$	$\pm m \pm 2, \pm m$
$\epsilon_{xz,zx,yz,zy}$	$l, l-2$	$\pm m \pm 1$	$l, l+2$	$\pm m \pm 1$
ϵ_{zz}	$l, l-2$	$\pm m$	$l, l+2$	$\pm m$

$$\begin{aligned}u_x =& R\sum_{m'=m\pm1}\left[A_{m'}(r^2 - R^2)r^{l-1}Y_{l-1}^{m'} + B_{m'}r^{l+1}Y_{l+1}^{m'}\right.\\ &\left. + C_{m'}r^{l-1}Y_{l-1}^{m'}\right] + \text{c.c.},\end{aligned} \tag{27}$$

$$\begin{aligned}u_y =& R\sum_{m'=m\pm1}\left[D_{m'}(r^2 - R^2)r^{l-1}Y_{l-1}^{m'} + E_{m'}r^{l+1}Y_{l+1}^{m'}\right.\\ &\left. + F_{m'}r^{l-1}Y_{l-1}^{m'}\right] + \text{c.c.},\end{aligned} \tag{28}$$

$$u_z = R\left[G(r^2 - R^2)r^{l-1}Y_{l-1}^m + Hr^{l+1}Y_{l+1}^m + Ir^{l-1}Y_{l-1}^m\right] + \text{c.c.}, \tag{29}$$

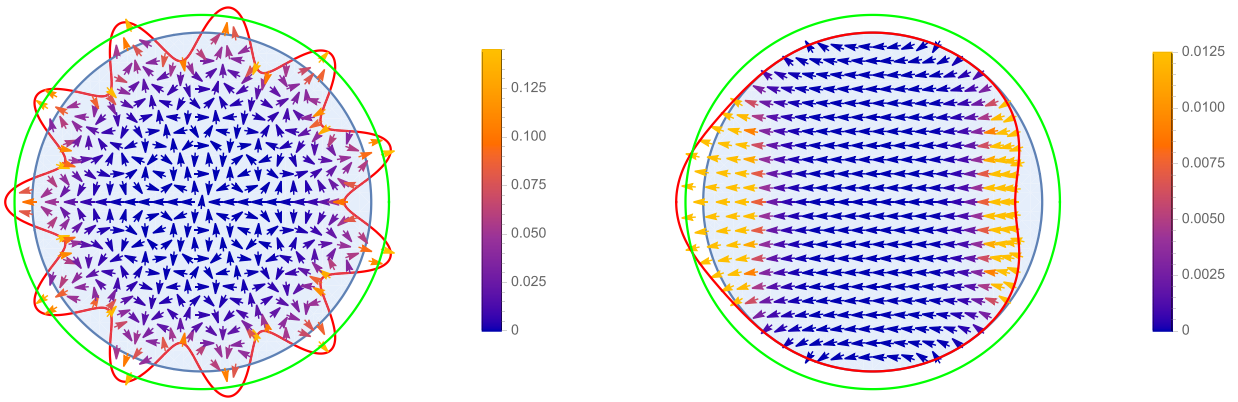

FIG. 1. Plot of the shape and displacement field within the xy plane (left) and the xz plane (right) of a sphere with a surface deformation given by a spherical harmonic with degree $l = 11$ and index $m = 11$ and $\nu = 0.3$. The direction of the arrows represents the direction of the elastic displacements within the sphere. The color of the arrows represents the magnitude of these displacements. The buckled shape, represented by the red curve, has a spherical harmonic amplitude of $g = 0.20$, corresponding to the excess area at the transition from the isotropically expanded phase to the buckled phase (Sec. VII). The smaller blue circle represents the undeformed sphere. The larger green circle represents the isotropically expanded sphere with the same surface area as the buckled shape.

where the coefficients ($A_{m'}$, $B_{m'}$, etc.) are all known functions of l, m, R, g, and ν and are given in Appendix C. It turns out that the coefficients vanish for all terms of the form $(r^2 - R^2)Y^{m'}_{l-3}$ that would otherwise appear in Eqs. (27), (28), and (29).

The displacement field ($\mathbf{u}$) for a sphere with a spherical harmonic surface deformation with $l = 11$ and $m = 11$ is illustrated in Fig. 1 for $g = 0.20$ and $\nu = 0.3$. This representation shows how the interior of the original sphere (blue, smaller circle) is deformed to the buckled shape (red curve). The larger green circle has the same surface area as the buckled shape and is included for reference.

V. SPHERICAL VOIDS WITH A SPHERICAL HARMONIC SHAPE DEFORMATION

Similar to Sec. IV, our solution for spherical voids is

$$v_x = R\sum_{m'=m\pm1}\left[J_{m'}(r^2-R^2)r^{-2-l}Y^{m'}_{l+1} + K_{m'}r^{-l}Y^{m'}_{l-1} + L_{m'}r^{-2-l}Y^{m'}_{l+1}\right] + \text{c.c.}, \tag{30}$$

$$v_y = R\sum_{m'=m\pm1}\left[M_{m'}(r^2-R^2)r^{-2-l}Y^{m'}_{l+1} + N_{m'}r^{-l}Y^{m'}_{l-1} + O_{m'}r^{-2-l}Y^{m'}_{l+1}\right] + \text{c.c.}, \tag{31}$$

$$v_z = R\left[P(r^2-R^2)r^{-2-l}Y^{m}_{l+1} + Qr^{-l}Y^{m}_{l-1} + Sr^{-2-l}Y^{m}_{l+1}\right] + \text{c.c.}, \tag{32}$$

where the coefficients here are given in Appendix D. The displacement field for a spherical void ($\mathbf{v}$) with a spherical harmonic surface deformation with $l = 12$ and $m = 12$ is similarly plotted in Fig. 2 for $\nu = 0.3$ and $g = 0.25$.

VI. BULK ELASTIC ENERGIES

Elasticity theory informs us that the elastic energy density, w, can be directly calculated from the derivatives of the displacement $\mathbf{u}$, namely the strains, $\epsilon_{ij} = \frac{1}{2}(\partial_i u_j + \partial_j u_i)$:

$$w = \mu\left[\frac{1-\nu}{1-2\nu}\left(\epsilon^2_{xx}+\epsilon^2_{yy}+\epsilon^2_{zz}\right) + \frac{2\nu}{1-2\nu}(\epsilon_{xx}\epsilon_{yy}+\epsilon_{yy}\epsilon_{zz} + \epsilon_{zz}\epsilon_{xx}) + 2\left(\epsilon^2_{xy}+\epsilon^2_{yz}+\epsilon^2_{zx}\right)\right]. \tag{33}$$

Then, to find the total bulk energy, W, we must integrate the energy density over the volume of the sphere (or over the volume outside the spherical void).

Using Eqs. (27), (28), and (29), in conjunction with Eqs. (A4), (A5), and (A6) from Appendix A, we can calculate each strain component with the result that each strain component comprises a sum of up to 20 spherical harmonics:

$$\epsilon_{ij} = \sum_{\substack{l'=l-2,l \\ m'=\pm m,\pm m\pm1,\pm m\pm2}} d_{l',m'}Y^{m'}_{l'}, \tag{34}$$

where $d_{l',m'}$ are the coefficients of $Y^{m'}_{l'}$ in ϵ_{ij} and depend on Cartesian coordinates i and j (Table I).

The spherical harmonics are orthogonal and normalized, that is,

$$\int Y^m_l\left(Y^{m'}_{l'}\right)^* d\Omega = \delta_{ll'}\delta_{mm'}, \tag{35}$$

where $(Y^m_l)^*$ is the complex conjugate of Y^m_l. Since $(Y^m_l)^* = (-1)^m Y^{-m}_l$, it follows that

$$\int Y^m_l Y^{-m'}_{l'} d\Omega = (-1)^m \delta_{ll'}\delta_{mm'}. \tag{36}$$

We can use this result to facilitate integration of the energy density over angles by first representing ϵ_{ij} as two vectors, each of 10 components, one corresponding to spherical harmonics of degree l and the other corresponding to spherical harmonics of degree $l-2$ (l and $l+2$ for irregular

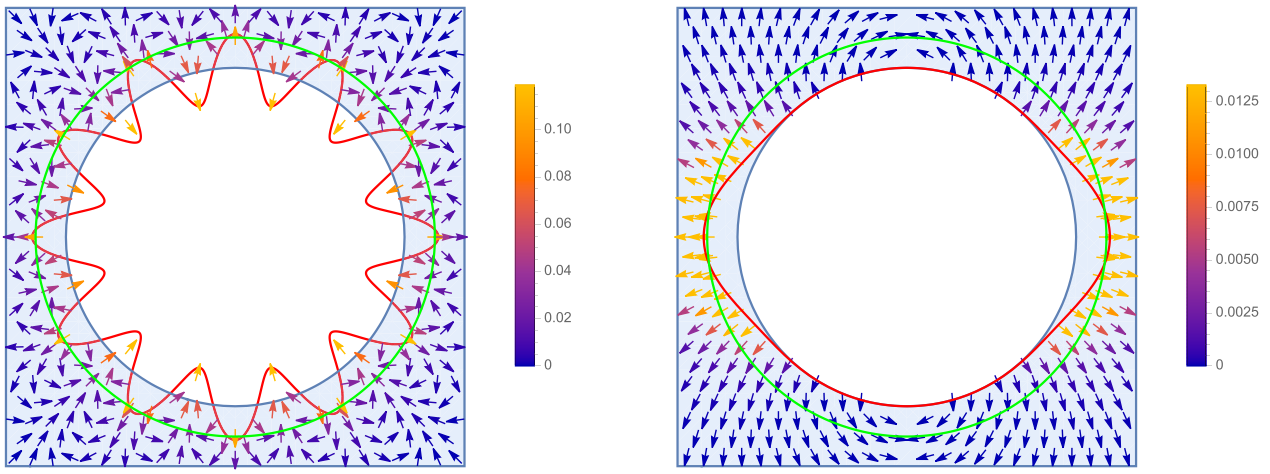

FIG. 2. Plot of the shape and displacement field within the xy plane (left) and the xz plane (right) of a spherical void with a surface deformation given by a spherical harmonic with degree $l = 12$ and index $m = 12$ and $\nu = 0.3$. The direction of the arrows represents the direction of the elastic displacements within the sphere. The color of the arrows represents the magnitude of these displacements. The buckled shape, represented by the red curve, has a spherical harmonic amplitude of $g = 0.25$, corresponding to the excess area at the transition from the isotropically expanded phase to the buckled phase (Sec. VII). The smaller blue circle represents the undeformed sphere. The larger green circle represents the isotropically expanded sphere with the same surface area as the buckled shape.

solution):

$$\mathbf{d}_{\epsilon_{ij}} = (d_{l',m+2}, d_{l',m+1}, d_{l',m}, d_{l',m-1}, d_{l',m-2}, d_{l',-m+2}, d_{l',-m+1}, d_{l',-m}, d_{l',-m-1}, d_{l',-m-2}), \tag{37}$$

where $l' = l - 2,\ l$. Next, for each of l and $l - 2$, we construct a 10×10 matrix, whose entries derive from the left hand side of Eq. (36):

$$M = \begin{pmatrix}
\delta_{-2,m} & 0 & -\delta_{-1,m} & 0 & \delta_{0,m} & 0 & 0 & 0 & 0 & (-1)^m \\
0 & \delta_{-1,m} & 0 & -\delta_{0,m} & 0 & 0 & 0 & 0 & (-1)^{m+1} & 0 \\
-\delta_{-1,m} & 0 & \delta_{0,m} & 0 & -\delta_{1,m} & 0 & 0 & (-1)^m & 0 & 0 \\
0 & -\delta_{0,m} & 0 & \delta_{1,m} & 0 & 0 & (-1)^{m+1} & 0 & 0 & 0 \\
\delta_{0,m} & 0 & -\delta_{1,m} & 0 & \delta_{2,m} & (-1)^m & 0 & 0 & 0 & 0 \\
0 & 0 & 0 & 0 & (-1)^m & \delta_{2,m} & 0 & -\delta_{1,m} & 0 & \delta_{0,m} \\
0 & 0 & 0 & (-1)^{m+1} & 0 & 0 & \delta_{1,m} & 0 & -\delta_{0,m} & 0 \\
0 & 0 & (-1)^m & 0 & 0 & -\delta_{1,m} & 0 & \delta_{0,m} & 0 & -\delta_{-1,m} \\
0 & (-1)^{m+1} & 0 & 0 & 0 & 0 & -\delta_{0,m} & 0 & \delta_{-1,m} & 0 \\
(-1)^m & 0 & 0 & 0 & 0 & \delta_{0,m} & 0 & -\delta_{-1,m} & 0 & \delta_{-2,m}
\end{pmatrix}. \tag{38}$$

It then follows that the required integrals over angles now correspond to matrix multiplication:

$$\int \epsilon_{ij}\epsilon_{pq} d\Omega = \mathbf{d}_{\epsilon_{ij}} M \mathbf{d}_{\epsilon_{pq}}{}^T, \tag{39}$$

where $\mathbf{d}_{\epsilon_{pq}}{}^T$ is the transpose of $\mathbf{d}_{\epsilon_{pq}}$. The integrals over r must be done explicitly:

$$\int_0^R \mathbf{d}_{\epsilon_{ij}} M \mathbf{d}_{\epsilon_{pq}}{}^T r^2 dr \tag{40}$$

for spheres and

$$\int_R^\infty \mathbf{d}_{\epsilon_{ij}} M \mathbf{d}_{\epsilon_{pq}}{}^T r^2 dr \tag{41}$$

for spherical voids. Even though several of the matrix elements of matrix M [Eq. (38)] explicitly depend on particular values of the spherical harmonic index, m, both the total elastic energy and the elastic energy within a shell at radius r are independent of m, that is, all shapes with the same l have the same energy. Because the expression for the elastic energy is invariant under rotations, we can understand the m independence of the elastic energy by realizing that with the given boundary conditions—a radial surface displacement with an amplitude proportional to a spherical harmonic—the elastic energy is a functional of the spherical-harmonic surface shape. Since each spherical harmonic is an irreducible representation of the rotation group, the elastic energy must therefore be independent of m.

For general values of l, the expression for the bulk elastic energy appears unwieldy (as can be seen from the MATHEMATICA notebook). However, for any specific value of l, the elastic energy reduces to a remarkably simple form. Examination of this energy for values of l from 1 to 25, using MATHEMATICA's `FindSequenceFunction`, indicates that the bulk elastic

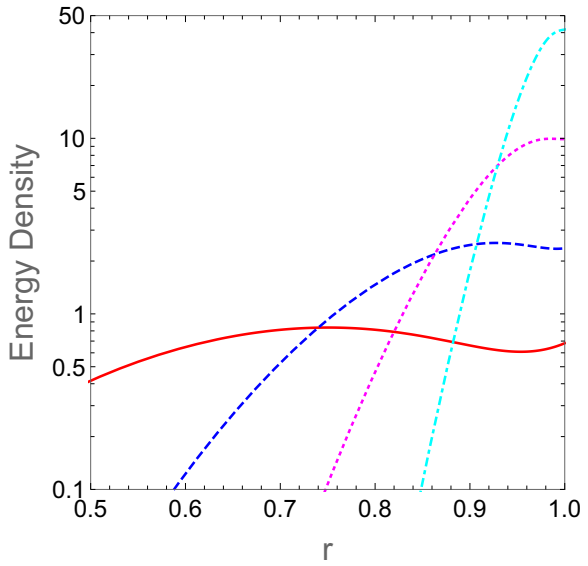

FIG. 3. Plot of the energy density as a function of r for $l = 4, 8, 16, 32$ for spheres. Red solid line corresponds to $l = 4$, blue dashed line corresponds to $l = 8$, magenta dotted line corresponds to $l = 16$, and cyan dot-dashed line corresponds to $l = 32$.

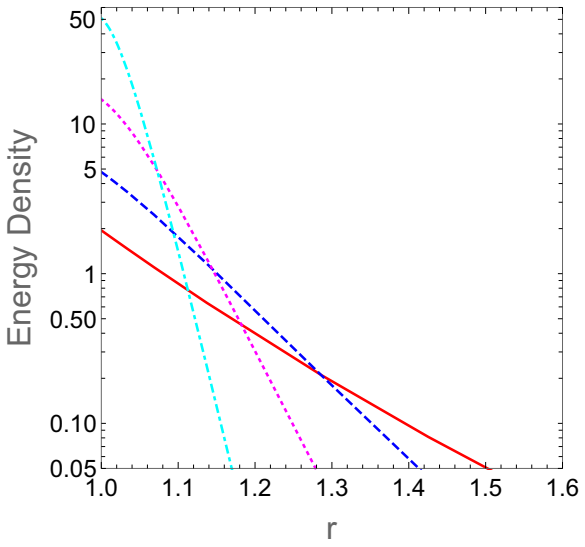

FIG. 4. Plot of the energy density as a function of r for $l = 4, 8, 16, 32$ for spherical voids. Red solid line corresponds to $l = 4$, blue dashed line corresponds to $l = 8$, magenta dotted line corresponds to $l = 16$, and cyan dot-dashed line corresponds to $l = 32$.

energies are given for general l by

$$W = g^2\mu R^3\left(\frac{(2l^2-3l-1)\nu-(2l^2-l+1)}{2(2l+1)\nu-(3l+1)}\right) \tag{42}$$

for spheres and

$$W = g^2\mu R^3\left(\frac{(4+7l+2l^2)\nu-(4+5l+2l^2)}{2(1+2l)\nu-(2+3l)}\right) \tag{43}$$

for spherical voids. Equations (42) and (43) are key results of this paper.

Figures 3 and 4 present the energy density, averaged over angles, within a shell at radius r for spheres and spherical voids, respectively. Inspection of Figs. 3 and 4 makes it clear that, for increasing l, most of the energy density, displacement, and strain is confined to an increasingly narrow near-surface layer. In Fig. 3 for spheres, each curve displays a peak at a radius less than R, which appears progressively closer to the surface for progressively larger l values. By contrast, in Fig. 4, the curves for spherical voids appear to decrease monotonically as r increases.

For boundary conditions, described by the sum of two spherical harmonics, Y_{lm} and $Y_{l'm'}$, the solution for the displacement $\mathbf{u}$ is the sum of the two solutions, satisfying boundary conditions described by Y_{lm} and $Y_{l'm'}$ separately. This result is inevitable given that Eq. (1) is linear in $\mathbf{u}$. We furthermore find that the corresponding bulk elastic energy is also additive, i.e., the energy for the two-spherical-harmonic boundary condition, $Y_{lm} + Y_{l'm'}$, is the sum of the energy for boundary condition, Y_{lm}, and the energy for boundary condition, $Y_{l'm'}$. This is because the solutions with different values of l and m are eigenfunctions that diagonalize the elastic energy.

Finally, as the alternatives to a buckled sphere and a buckled spherical void, we consider the elastic energy of an isotropically expanded sphere and an isotropically expanded spherical void. In the case of an isotropically expanded sphere, the displacement is $\mathbf{u} = g\mathbf{r}$ [which also satisfies Eq. (1)], so that $u_x = gx$, $u_y = gy$, $u_z = gz$, and $\epsilon_{xx} = \epsilon_{yy} = \epsilon_{zz} = g$, while $\epsilon_{ij} = 0$ for $i \neq j$. Substituting these results for the strains into Eq. (33), we find, for the energy density,

$$w = 3\mu g^2\frac{1+\nu}{1-2\nu} \tag{44}$$

and, for the total elastic energy of an isotropically expanded sphere,

$$E_{\text{isotropic}} = 4\pi R^3\mu g^2\frac{1+\nu}{1-2\nu}. \tag{45}$$

In the case of an isotropically expanded spherical void, the displacement is $\mathbf{u} = g\frac{R^3}{r^2}\mathbf{r}$. The corresponding energy density is

$$w = \frac{6\mu g^2R^6}{r^6} \tag{46}$$

and the corresponding total energy is

$$E_{\text{isotropic}} = 8\pi\mu g^2R^3. \tag{47}$$

VII. CORE-SHELL SYSTEM

In this section, we revisit the buckling instability that occurs in a spherical core-shell system, when the area mismatch between a stiff shell and a soft core exceeds a critical value, corresponding to the elastic energy of an isotropically expanded state exceeding the elastic energy of a buckled state. To generally treat a core-shell system, composed of two materials with different elastic properties, in addition to the regular solution applicable within the core, we would also need the solution to Eq. (1) within a spherical shell. The solution within a shell is the superposition of the regular and the irregular

solutions, which must then together be matched to the appropriate boundary conditions at the inner radius, where the core and the shell meet, and at the outer radius of the shell. With these solutions in hand, we would then calculate the strains and elastic energies.

Instead of this route, we follow Ref. [19] and consider the limiting case that the shell can be described as a thin membrane of fixed area, A, and bending stiffness, κ. The surface energy is calculated by integrating the square of the mean curvature, H, over the surface:

$$E_{\text{surface}} = \frac{\kappa}{2}\oint_{r=R} H^2 dS. \tag{48}$$

Then, when the shape of the membrane is described by a real spherical harmonic, Y_{lm}, the l-dependent part of the membrane elastic energy is

$$E_{\text{surface}} = \frac{\kappa}{8} g^2 [l(l+2)(l^2-1)], \tag{49}$$

independent of m [19,25].

In the context of a fixed-area membrane, the buckling instability is controlled by relative excess area, namely the difference between the area of the membrane and the area of the spherical core, normalized by the area of the core:

$$\Delta = \frac{A}{4\pi R^2} - 1. \tag{50}$$

Therefore, we must relate the buckling amplitude, g, to the relative excess area, Δ. For buckled shapes, described by real spherical harmonics, Y_{lm}, Ref. [19] showed that

$$g = \sqrt{\Delta}\left(\frac{8\pi}{l(l+1)+2}\right)^{1/2}. \tag{51}$$

In this case, the energies of both the core and the shell are proportional to g^2. Therefore, the total energy of the core-shell system with shape Y_{lm} is proportional to Δ.

Combining Eqs. (42), (49), and (51) and introducing α, given by

$$\alpha = \frac{\mu R^3}{\kappa}, \tag{52}$$

we find that the total core-shell energy for spheres is

$$E_{\text{total}} = \frac{8\kappa\Delta}{l^2+l+2}\pi\left(\alpha\frac{(2l^2-3l-1)\nu-(2l^2-l+1)}{2(2l+1)\nu-(3l+1)} + \frac{1}{8}(l-1)l(l+1)(l+2)\right). \tag{53}$$

Similarly, the total energy for spherical voids, with a membrane surrounding the void, is

$$E_{\text{total}} = \frac{8\kappa\Delta}{l^2+l+2}\pi\left(\alpha\frac{(4+7l+2l^2)\nu-(4+5l+2l^2)}{2(1+2l)\nu-(2+3l)} + \frac{1}{8}(l-1)l(l+1)(l+2)\right). \tag{54}$$

Figures 5 and 6 plot these energies for $\nu = 0.2$. In these plots, each line represents the energy associated with a particular value of l. It is clear from these figures that which value of l corresponds to the lowest energy steps from one value to the next as α increases. The l value of the lowest

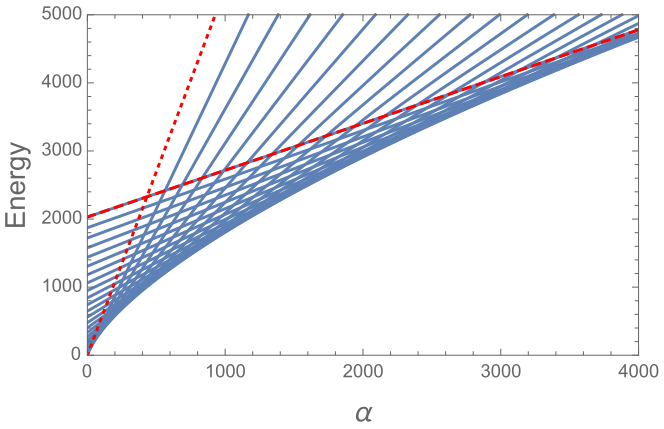

FIG. 5. Plot of energy as a function of α for different l values for the solution for spheres. Red dotted and dashed lines correspond to $l = 1$ and $l = 25$. Other lines correspond to $l = 2, 3, 4, \ldots, 24$ in order of increasing distance from the red dotted line for $l = 1$. $\nu = 0.2$.

total energy state is plotted versus α in Fig. 7 for spheres and in Fig. 8 for spherical voids. As α increases, the minimum energy l increases. We pick four values of Poisson's ratio ν to illustrate the trend. Poisson's ratio is the material property describing the deformation of a material in directions perpendicular to the direction of loading, which lies between -1 and $\frac{1}{2}$ for stable, isotropic, linear elastic material. A Poisson's ratio of $\frac{1}{2}$ means that the material is incompressible.

To further make sense of Fig. 7, we consider the limit of large l and treat l as a continuous variable. Then, for spheres

$$E_{\text{total}} \simeq 8\kappa\Delta\left(\frac{2\alpha(1-\nu)}{(3-4\nu)l} + \frac{l^2}{8}\right), \tag{55}$$

and we can find the value of l that minimizes the total energy (l^*). The result is

$$l^* = 2\left(\frac{\alpha(1-\nu)}{3-4\nu}\right)^{\frac{1}{3}}. \tag{56}$$

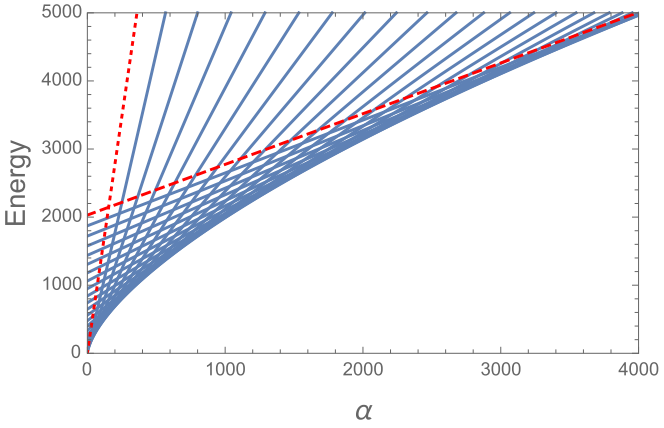

FIG. 6. Plot of energy as a function of α for different l values for the solution for spherical voids. Red dotted and dashed lines correspond to $l = 1$ and $l = 25$. Other lines correspond to $l = 2, 3, 4, \ldots, 24$ in order of increasing distance from the red dotted line for $l = 1$. $\nu = 0.2$.

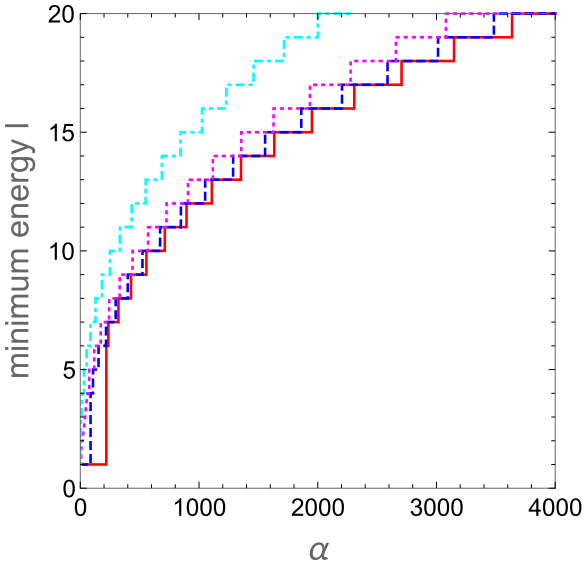

FIG. 7. Plot of l of the lowest energy state as a function of α for four different values of $\nu = -0.1, 0, 0.2, 0.5$ for the solution for spheres. Red solid line corresponds to $\nu = -0.1$, blue dashed line corresponds to $\nu = 0$, magenta dotted line corresponds to $\nu = 0.2$, and cyan dot-dashed line corresponds to $\nu = 0.5$.

The value of l^* varies as $\alpha^{\frac{1}{3}}$, consistent with the behavior apparent in Fig. 7. The elastic energy corresponding to l^* is

$$E^*_{\text{total}} = 12\kappa\Delta\left(\frac{\alpha(1-\nu)}{3-4\nu}\right)^{\frac{2}{3}}, \tag{57}$$

reminiscent of the minimum energy envelope in Fig. 5.

For the isotropically expanded state, $g = \Delta/2$ to linear order. Therefore, in contrast to the linear-in-Δ buckled state

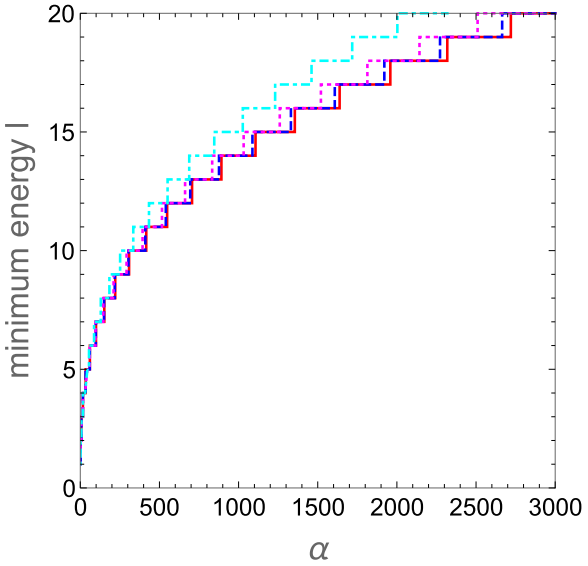

FIG. 8. Plot of l of the lowest energy state as a function of α for four different values of $\nu = -0.1, 0, 0.2, 0.5$ for the solution for spherical voids. Red solid line corresponds to $\nu = -0.1$, blue dashed line corresponds to $\nu = 0$, magenta dotted line corresponds to $\nu = 0.2$, and cyan dot-dashed line corresponds to $\nu = 0.5$.

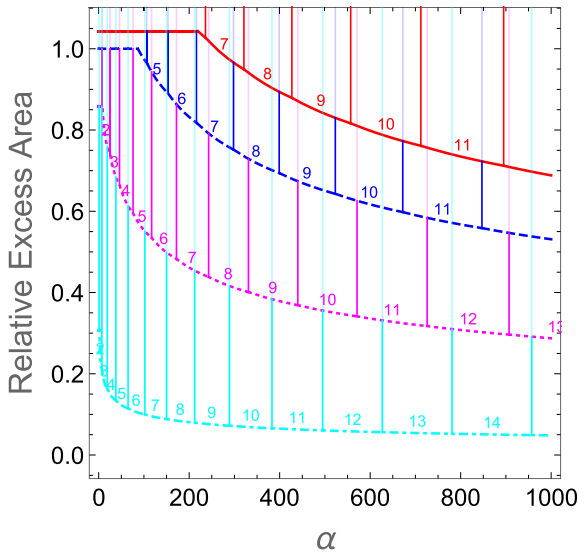

FIG. 9. Sphere phase diagram for four different values of $\nu = -0.1, 0, 0.2, 0.45$. The red solid line corresponds to $\nu = -0.1$, the blue dashed line corresponds to $\nu = 0$, the magenta dotted line corresponds to $\nu = 0.2$, and the cyan dot-dashed line corresponds to $\nu = 0.45$. In each case, the region above these curved lines is the spherical-harmonic phase and the region below the curve is the isotropic-expansion phase. The vertical lines separate regions with different values of l.

energy, the energy of an isotropically expanded sphere is

$$E_{\text{isotropic}} = \pi R^3 \mu \Delta^2 \frac{1+\nu}{1-2\nu}, \tag{58}$$

proportional to Δ^2. Thus, for small Δ, the isotropic state inevitably has a lower energy than the buckled state, while, for large Δ, the opposite is true.

To find the critical value of Δ at which the core-shell system transitions from isotropically expanded to buckled, we set the energies for both cases to be equal and then solve for the corresponding value of Δ, namely Δ_c:

$$\Delta_c = \frac{E_{\text{total}}}{\pi R^3 \mu \frac{1+\nu}{1-2\nu}\Delta_c} = \frac{E_{\text{total}}/(\kappa\Delta_c)}{\pi\alpha\frac{1+\nu}{1-2\nu}}. \tag{59}$$

Since $E_{\text{total}}/(\kappa\Delta_c)$ is independent of Δ_c, the right-hand side of Eq. (59) is the desired solution for Δ_c. The analogous result for spherical voids with an interior shell is

$$\Delta_c = \frac{E_{\text{total}}/(\kappa\Delta_c)}{2\pi\alpha}. \tag{60}$$

The deformations shown in Fig. 1 and Fig. 2 for spheres and spherical voids, respectively, both correspond to Δ_c for $\alpha = 600$. We plot Δ_c as a function of α as the curved lines in Fig. 9 for spheres and in Fig. 10 for spherical voids. The region below the Δ_c-versus-α curve corresponds to an isotropically expanded phase, while the region above is the buckled phase. The vertical lines in these figures separate buckled phases with different l values. Thus Figs. 9 and 10 represent shape phase diagrams.

In general, a larger value of α requires a lower relative excess area in order for there to be a transition into the buckled

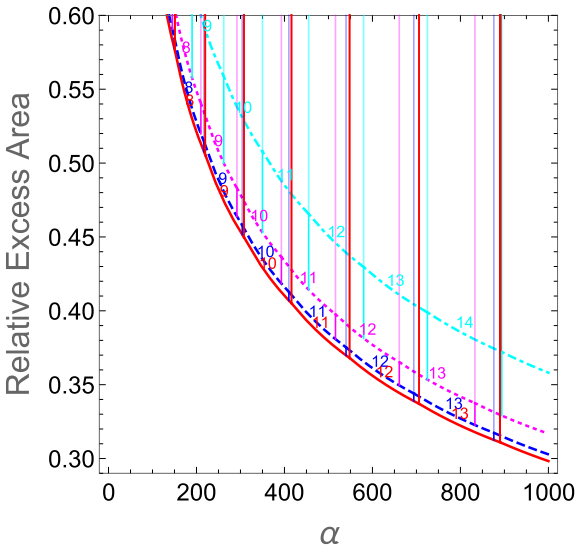

FIG. 10. Spherical void phase diagram for four different values of $\nu = -0.1, 0, 0.2, 0.45$. The red solid line corresponds to $\nu = -0.1$, the blue dashed line corresponds to $\nu = 0$, the magenta dotted line corresponds to $\nu = 0.2$, and the cyan dot-dashed line corresponds to $\nu = 0.45$. In each case, the region above these curved lines is the spherical-harmonic phase and the region below the curve is the isotropic-expansion phase. The vertical lines separate regions with different values of l.

phase above the Δ_c curve. A larger value of α also gives rise to a larger l value in the buckled phase. Clearly, the vertical lines separating buckled states with different values of l do not align at the same values of α for different Poisson ratios. In the large-l limit, for a core-shell system, we have that

$$\Delta_c = \frac{12}{\pi}\alpha^{-\frac{1}{3}}\left(\frac{1-2\nu}{1+\nu}\right)\left(\frac{1-\nu}{3-4\nu}\right)^{\frac{2}{3}}. \tag{61}$$

To realize our results for the buckled phase quantitatively, linear elasticity must be applicable. The maximum strains at the phase boundaries are l dependent, but typically are about 0.6 for spheres and about 3 for voids. In comparison, the range of linear behavior for rubber, for example, extends to strains of about 1, suggesting that rubber-filled core shells could realize our theory quantitatively, but that voids even in rubber would not.

VIII. CONCLUSION

By applying linear elasticity theory and exploiting well-known properties of the solid harmonics, we have described how to find the displacements either inside solid spheres or outside spherical voids, assuming in both cases that the surface of the sphere or the void shows a radial surface deformations, whose amplitude is given by a real spherical harmonic. Using the displacements so obtained, we then calculated the corresponding bulk elastic energies, providing closed-form expressions for these energies, for any values of the spherical harmonic degree (l), Poisson ratio, and shear modulus. We found that the elastic energies are independent of the spherical harmonic index (m), consistent with expectations based on symmetry considerations. These collected results represent an important addition to our knowledge of the linear elasticity of systems with (near) spherical symmetry. In addition to their relevance to the buckling transitions of core-shell systems, because any shape can be described as a superposition of spherical harmonics, our results will be valuable for researchers broadly interested in the elasticity of spheres or spherical voids that experience surface shape deformations. We also revisited the buckling instability experienced by a core-shell system comprising an elastic sphere, attached within a membrane of fixed area, that occurs when the area of the membrane sufficiently exceeds the area of the unstrained sphere. By finding the state which possesses the smallest total energy the sum of the bulk and surface elastic energies within linear elasticity, we determined the phase diagram of the core-shell sphere's shape, specifying what value of l is realized as a function of the area mismatch and the core-shell elasticity. Similarly, we also determined the shape phase diagram for a spherical void bounded by a fixed-area membrane.

A MATHEMATICA notebook that performs the calculations described is available as Supplemental Material [24].

ACKNOWLEDGMENTS

This work was supported by an Allen Distinguished Investigator Award, a Paul G. Allen Frontiers Group advised grant of the Paul G. Allen Family Foundation. We are especially grateful to D. Poland for finding the simple form of the bulk energy for general values of l and N. Read for invaluable discussions.

APPENDIX A: PROPERTIES OF REGULAR SOLID HARMONICS

We summarize some useful results:

$$\nabla^2\left(r^l Y_l^m\right) = 0, \tag{A1}$$

$$\nabla\cdot\left(r^2\nabla\left(r^l Y_l^m\right)\right) = (\nabla r^2)\cdot\nabla\left(r^l Y_l^m\right) = 2\mathbf{r}\cdot\nabla\left(r^l Y_l^m\right) = 2r\frac{\partial}{\partial r}\left(r^l Y_l^m\right) = 2l\left(r^l Y_l^m\right), \tag{A2}$$

$$\nabla^2\left(r^2\nabla\left(r^l Y_l^m\right)\right) = 2(2l+1)\nabla\left(r^l Y_l^m\right), \tag{A3}$$

$$\frac{\partial}{\partial x}\left(r^l Y_l^m\right) = \frac{1}{2}r^{l-1}\sqrt{\frac{(2l+1)(l-m)!}{(l+m)!}}\left(\frac{Y_{l-1}^{m+1}}{\sqrt{\frac{(2l-1)(l-m-2)!}{(l+m)!}}} - \frac{(l+m-1)(l+m)Y_{l-1}^{m-1}}{\sqrt{\frac{(2l-1)(l-m)!}{(l+m-2)!}}}\right), \tag{A4}$$

$$\frac{\partial}{\partial y}\left(r^l Y_l^m\right) = -\frac{1}{2} i r^{l-1} \sqrt{\frac{(2l+1)(l-m)!}{(l+m)!}} \left(\frac{(l+m-1)(l+m) Y_{l-1}^{m-1}}{\sqrt{\frac{(2l-1)(l-m)!}{(l+m-2)!}}} + \frac{Y_{l-1}^{m+1}}{\sqrt{\frac{(2l-1)(l-m-2)!}{(l+m)!}}} \right), \tag{A5}$$

and

$$\frac{\partial}{\partial z}\left(r^l Y_l^m\right) = \frac{(l+m) r^{l-1} \sqrt{\frac{(2l+1)(l-m)!}{(l+m)!}} Y_{l-1}^m}{\sqrt{\frac{(2l-1)(l-m-1)!}{(l+m-1)!}}}. \tag{A6}$$

It follows that

$$\alpha = \frac{(b_x - i b_y) \sqrt{\frac{(2l+3)(l-m+1)!}{(l+m+1)!}}}{2\sqrt{\frac{(2l+1)(l-m-1)!}{(l+m+1)!}}}, \tag{A7}$$

$$\beta = \frac{b_z (l+m+1) \sqrt{\frac{(2l+3)(l-m+1)!}{(l+m+1)!}}}{\sqrt{\frac{(2l+1)(l-m)!}{(l+m)!}}}, \tag{A8}$$

and

$$\gamma = -\frac{(b_x + i b_y)(l+m)(l+m+1) \sqrt{\frac{(2l+3)(l-m+1)!}{(l+m+1)!}}}{2\sqrt{\frac{(2l+1)(l-m+1)!}{(l+m-1)!}}}. \tag{A9}$$

APPENDIX B: PROPERTIES OF IRREGULAR SOLID HARMONICS

$$\frac{\partial}{\partial x}\left(r^{-l-1} Y_l^m\right) = \frac{1}{2}\sqrt{\frac{2l+1}{2l+3}} \left(\sqrt{(l+m+1)(l+m+2)} r^{-l-2} Y_{l+1}^{m+1} - \sqrt{(l-m+1)(l-m+2)} r^{-l-2} Y_{l+1}^{m-1} \right), \tag{B1}$$

$$\frac{\partial}{\partial y}\left(r^{-l-1} Y_l^m\right) = -\frac{1}{2} i \sqrt{\frac{2l+1}{2l+3}} \left(\sqrt{(l-m+1)(l-m+2)} r^{-l-2} Y_{l+1}^{m-1} + \sqrt{(l+m+1)(l+m+2)} r^{-l-2} Y_{l+1}^{m+1} \right), \tag{B2}$$

$$\frac{\partial}{\partial z}\left(r^{-l-1} Y_l^m\right) = -\sqrt{\frac{2l+1}{2l+3}} \sqrt{(l-m+1)(l+m+1)} r^{-l-2} Y_{l+1}^m. \tag{B3}$$

APPENDIX C: REGULAR SOLUTION COEFFICIENTS

$$A_{m+1} = \begin{cases} 0, & l < m+2, \\ \frac{g(l+1)(2l+3) e^{2i\pi(l+m)} R^{-l-1} \Gamma(l-m+1)}{4\sqrt{2}[l(4\nu-3)+2\nu-1]\sqrt{(4l^2-1)(l-m)!\Gamma(l-m-1)}}, & \text{otherwise}, \end{cases} \tag{C1}$$

$$A_{m-1} = \begin{cases} \frac{g(-1)^{-2l}\sqrt{\frac{(l+m-1)(l+m)}{8l^2-2}} R^{-l-1}\left[-(l+1)(2l+3) e^{2i\pi(2l+m)}\right]}{4[l(4\nu-3)+2\nu-1]}, & l+m \geqslant 2, \\ 0, & \text{otherwise}, \end{cases} \tag{C2}$$

$$B_{m+1} = -\frac{1}{2} g(-1)^{2(l+m)} \sqrt{\frac{(l+m+1)(l+m+2)}{8l(l+2)+6}} R^{-l-1}, \tag{C3}$$

$$B_{m-1} = \frac{1}{2} g(-1)^{2(l+m)} \sqrt{\frac{(l-m+1)(l-m+2)}{8l(l+2)+6}} R^{-l-1}, \tag{C4}$$

$$C_{m+1} = \begin{cases} \frac{1}{2} g(-1)^{-2l} \sqrt{\frac{(l-m-1)(l-m)}{8l^2-2}} R^{l+1} (R^2)^{-l}, & l \geqslant m+2, \\ 0, & \text{otherwise}, \end{cases} \tag{C5}$$

$$C_{m-1} = \begin{cases} -\frac{1}{2} g(-1)^{-2l} \sqrt{\frac{(l+m-1)(l+m)}{8l^2-2}} R^{l+1} (R^2)^{-l}, & l+m \geqslant 2, \\ 0, & \text{otherwise}, \end{cases} \tag{C6}$$

$$D_{m+1}=\begin{cases}\frac{1}{8(2l+1)^2[l(4\nu-3)+2\nu-1]\sqrt{l[8l(l+1)-6]\Gamma(l-m-1)}}\big(ig(-1)^m e^{i\pi(3l+m)}(-R)^{-l-1}\\ \times\big\{l^2\sqrt{l(2l+1)^3(2l+3)\Gamma(l-m+1)}+l[2m\sqrt{l(2l+1)^3(2l+3)\Gamma(l-m+1)}\\ +3\sqrt{l(2l+1)^3(2l+3)\Gamma(l-m+1)}+2\sqrt{l(2l+1)^3(2l+3)(l-m+1)\Gamma(l-m+2)}\\ +2\sqrt{l(2l+1)(2l+3)(l-m+1)(l-m+2)\Gamma(l-m+3)}]+2\sqrt{l(2l+1)^3(2l+3)\Gamma(l-m+1)} & l\geqslant m+2,\\ +2\sqrt{l(2l+1)^3(2l+3)(l-m+1)\Gamma(l-m+2)}+m[m\sqrt{l(2l+1)^3(2l+3)\Gamma(l-m+1)}\\ +3\sqrt{l(2l+1)^3(2l+3)\Gamma(l-m+1)}+2\sqrt{l(2l+1)^3(2l+3)(l-m+1)\Gamma(l-m+2)}]\\ +\sqrt{l(2l+1)(2l+3)(l-m+1)(l-m+2)\Gamma(l-m+3)}\big\}\big),\\ 0, & \text{otherwise},\end{cases} \tag{C7}$$

$$D_{m-1}=\begin{cases}\dfrac{ig(l+1)(2l+3)e^{i\pi(3l+2m)}\sqrt{\frac{(l+m-1)(l+m)}{8l^2-2}}(-R)^{-l-1}}{4[l(4\nu-3)+2\nu-1]}, & l+m\geqslant 2,\\ 0, & \text{otherwise},\end{cases} \tag{C8}$$

$$E_{m+1}=\frac{1}{2}ig(-1)^{2(l+m)}\sqrt{\frac{(l+m+1)(l+m+2)}{8l(l+2)+6}}R^{-l-1}, \tag{C9}$$

$$E_{m-1}=\frac{1}{2}ig(-1)^{2(l+m)}\sqrt{\frac{(l-m+1)(l-m+2)}{8l(l+2)+6}}R^{-l-1}, \tag{C10}$$

$$F_{m+1}=\begin{cases}-\frac{1}{2}ig(-1)^{-2l}\sqrt{\frac{(l-m-1)(l-m)}{8l^2-2}}R^{l+1}(R^2)^{-l}, & l\geqslant m+2,\\ 0, & \text{otherwise},\end{cases} \tag{C11}$$

$$F_{m-1}=\begin{cases}-\frac{1}{2}ig(-1)^{-2l}\sqrt{\frac{(l+m-1)(l+m)}{8l^2-2}}R^{l+1}(R^2)^{-l}, & l+m\geqslant 2,\\ 0, & \text{otherwise},\end{cases} \tag{C12}$$

$$I=\begin{cases}g(-1)^{-2l}\sqrt{\frac{(l-m)(l+m)}{8l^2-2}}R^{l+1}(R^2)^{-l}, & l\geqslant m+1,\\ 0, & \text{otherwise},\end{cases} \tag{C13}$$

$$H=g(-1)^{2(l+m)}\sqrt{\frac{(l-m+1)(l+m+1)}{8l(l+2)+6}}R^{-l-1}, \tag{C14}$$

$$G=\begin{cases}\frac{1}{4\sqrt{2}[l(4\nu-3)+2\nu-1]\sqrt{(2l-1)\Gamma(l-m)\Gamma(l+m)}}\big[g(-1)^{2(l+m)}R^{-l-1}\\ \times\big([(l+m+1)(l+m+2)]^{3/2}\Gamma(l+m+1)\sqrt{\frac{\Gamma(l-m+1)}{(2l+1)\Gamma(l+m+3)}}\\ +\sqrt{\frac{(l-m+1)(l-m+2)\Gamma(l-m+3)\Gamma(l+m+1)}{2l+1}}+2\sqrt{\frac{(l-m+1)(l+m+1)\Gamma(l-m+2)\Gamma(l+m+2)}{2l+1}}\big)\big], & l\geqslant m+1\\ 0, & \text{otherwise}.\end{cases}, \tag{C15}$$

APPENDIX D: IRREGULAR SOLUTION COEFFICIENTS

$$\begin{aligned}J_{m+1}=&\frac{1}{8(4l\nu-3l+2\nu-2)}g(-1)^{m-l}\sqrt{\frac{(l+m+1)(l+m+2)}{4l(l+2)+3}}R^l\Bigg[\sqrt{l(4l^2-1)(l-m-1)(l-m)}\\ &\times\left(\begin{cases}(-1)^{-l-m}\sqrt{\frac{(l-m-1)(l-m)}{8l^3-2l}}, & l\geqslant m+2\\ 0, & \text{otherwise}\end{cases}\right)\\ &+\sqrt{2}\sqrt{l(4l^2-1)(l-m)(l+m)}\left(\begin{cases}(-1)^{-l-m}\sqrt{-\frac{(l-m)(l+m)}{l-4l^3}}, & l\geqslant m+1\\ 0, & \text{otherwise}\end{cases}\right)\\ &+\sqrt{l(4l^2-1)(l+m-1)(l+m)}\left(\begin{cases}(-1)^{-l-m}\sqrt{\frac{(l+m-1)(l+m)}{8l^3-2l}}, & l+m\geqslant 2\\ 0, & \text{otherwise}\end{cases}\right)\Bigg],\end{aligned} \tag{D1}$$

$$J_{m-1}=\begin{cases}\frac{g(-1)^{-2l}(1-2l)l\sqrt{\frac{(l-m+1)(l-m+2)}{8l(l+2)+6}}R^l}{4(4l\nu-3l+2\nu-2)}, & l\geqslant m+2,\\ -\frac{g(-1)^{-2l}\sqrt{\frac{(l-m+1)(l-m+2)}{8l(l+2)+6}}(3l-m-1)(l+m)R^l}{8(4l\nu-3l+2\nu-2)}, & l\geqslant m+1\wedge l+m\geqslant 2,\\ -\frac{g(-1)^{-2l}(l-m)\sqrt{\frac{(l-m+1)(l-m+2)}{8l(l+2)+6}}(l+m)R^l}{4(4l\nu-3l+2\nu-2)}, & l\geqslant m+1,\\ -\frac{g(-1)^{-2l}\sqrt{\frac{(l-m+1)(l-m+2)}{8l(l+2)+6}}(l+m-1)(l+m)R^l}{8(4l\nu-3l+2\nu-2)}, & l+m\geqslant 2,\end{cases} \tag{D2}$$

$$K_{m+1}=\begin{cases}\frac{1}{2}g(-1)^{-2l}\sqrt{\frac{(l-m-1)(l-m)}{8l^2-2}}R^l, & l\geqslant m+2,\\ 0, & \text{otherwise},\end{cases} \tag{D3}$$

$$K_{m-1}=\begin{cases}-\frac{1}{2}g(-1)^{-2l}\sqrt{\frac{(l+m-1)(l+m)}{8l^2-2}}R^l, & l+m\geqslant 2,\\ 0, & \text{otherwise},\end{cases} \tag{D4}$$

$$L_{m+1}=-\frac{1}{2}g(-1)^{2(l+m)}\sqrt{\frac{(l+m+1)(l+m+2)}{8l(l+2)+6}}R^{l+2}, \tag{D5}$$

$$L_{m-1}=\frac{g(-1)^{2(l+m)}R^{l+2}}{2\sqrt{\frac{8l(l+2)+6}{(l-m+1)(l-m+2)}}}, \tag{D6}$$

$$\begin{aligned}M_{m+1}=&-\frac{1}{8(4l\nu-3l+2\nu-2)}ig(-1)^{m-l}\sqrt{\frac{(l+m+1)(l+m+2)}{4l(l+2)+3}}R^l\Bigg[\sqrt{l(4l^2-1)(l-m-1)(l-m)}\\&\times\left(\begin{cases}(-1)^{-l-m}\sqrt{\frac{(l-m-1)(l-m)}{8l^3-2l}}, & l\geqslant m+2\\ 0, & \text{otherwise}\end{cases}\right)\\&+\sqrt{2}\sqrt{l(4l^2-1)(l-m)(l+m)}\left(\begin{cases}(-1)^{-l-m}\sqrt{-\frac{(l-m)(l+m)}{l-4l^3}}, & l\geqslant m+1\\ 0, & \text{otherwise}\end{cases}\right)\\&+\sqrt{l(4l^2-1)(l+m-1)(l+m)}\left(\begin{cases}(-1)^{-l-m}\sqrt{\frac{(l+m-1)(l+m)}{8l^3-2l}}, & l+m\geqslant 2\\ 0, & \text{otherwise}\end{cases}\right)\Bigg],\end{aligned} \tag{D7}$$

$$\begin{aligned}M_{m-1}=&-\frac{1}{8(4l\nu-3l+2\nu-2)}ig(-1)^{m-l}R^l\Bigg[\sqrt{\frac{l(2l-1)(l-m-1)(l-m)(l-m+1)(l-m+2)}{2l+3}}\\&\times\left(\begin{cases}(-1)^{-l-m}\sqrt{\frac{(l-m-1)(l-m)}{8l^3-2l}}, & l\geqslant m+2\\ 0, & \text{otherwise}\end{cases}\right)\\&+\sqrt{2}\sqrt{\frac{l(2l-1)(l-m)(l-m+1)(l-m+2)(l+m)}{2l+3}}\left(\begin{cases}(-1)^{-l-m}\sqrt{-\frac{(l-m)(l+m)}{l-4l^3}}, & l\geqslant m+1\\ 0, & \text{otherwise}\end{cases}\right)\\&+\sqrt{\frac{l(2l-1)(l-m+1)(l-m+2)(l+m-1)(l+m)}{2l+3}}\left(\begin{cases}(-1)^{-l-m}\sqrt{\frac{(l+m-1)(l+m)}{8l^3-2l}}, & l+m\geqslant 2\\ 0, & \text{otherwise}\end{cases}\right)\Bigg],\end{aligned} \tag{D8}$$

$$N_{m+1}=\begin{cases}-\frac{1}{2}ig(-1)^{-2l}\sqrt{\frac{(l-m-1)(l-m)}{8l^2-2}}R^l, & l\geqslant m+2,\\ 0, & \text{otherwise},\end{cases} \tag{D9}$$

$$N_{m-1}=\begin{cases}-\frac{1}{2}ig(-1)^{-2l}\sqrt{\frac{(l+m-1)(l+m)}{8l^2-2}}R^l, & l+m\geqslant 2,\\ 0, & \text{otherwise},\end{cases} \tag{D10}$$

$$O_{m+1}=\frac{1}{2}ig(-1)^{2(l+m)}\sqrt{\frac{(l+m+1)(l+m+2)}{8l(l+2)+6}}R^{l+2}, \tag{D11}$$

$$O_{m-1}=\frac{ig(-1)^{2(l+m)}R^{l+2}}{2\sqrt{\frac{8l(l+2)+6}{(l-m+1)(l-m+2)}}}, \tag{D12}$$

$$S = g(-1)^{2(l+m)}\sqrt{\frac{(l-m+1)(l+m+1)}{8l(l+2)+6}}R^{l+2}, \tag{D13}$$

$$Q = \begin{cases} g(-1)^{-2l}\sqrt{\frac{(l-m)(l+m)}{8l^2-2}}R^l, & l \geqslant m+1, \\ 0, & \text{otherwise}, \end{cases} \tag{D14}$$

$$P = \begin{cases} -\frac{g(-1)^{-2l}l(2l-1)\sqrt{\frac{(l-m+1)(l+m+1)}{8l(l+2)+6}}R^l}{2(4lv-3l+2v-2)}, & l \geqslant m+2, \\ -\frac{g(-1)^{-2l}(3l-m-1)(l+m)\sqrt{\frac{(l-m+1)(l+m+1)}{8l(l+2)+6}}R^l}{4(4lv-3l+2v-2)}, & l \geqslant m+1 \wedge l+m \geqslant 2, \\ -\frac{g(-1)^{-2l}(l-m)(l+m)\sqrt{\frac{(l-m+1)(l+m+1)}{8l(l+2)+6}}R^l}{2(4lv-3l+2v-2)}, & l \geqslant m+1, \\ -\frac{g(-1)^{-2l}(l+m-1)(l+m)\sqrt{\frac{(l-m+1)(l+m+1)}{8l(l+2)+6}}R^l}{4(4lv-3l+2v-2)}, & l+m \geqslant 2. \end{cases} \tag{D15}$$

[1] J. Yin, Z. Cao, C. Li, I. Sheinman, and X. Chen, Stress-driven buckling patterns in spheroidal core/shell structures, Proc. Natl. Acad. Sci. USA **105**, 19132 (2008).

[2] J. Yin, X. Chen, and I. Sheinman, Anisotropic buckling patterns in spheroidal film/substrate systems and their implications in some natural and biological systems, J. Mech. Phys. Solids **57**, 1470 (2009).

[3] B. Li, F. Jia, Y.-P. Cao, X.-Q. Feng, and H. Gao, Surface Wrinkling Patterns on a Core-Shell Soft Sphere, Phys. Rev. Lett. **106**, 234301 (2011).

[4] M. L. Munguira, J. Martín, E. García-Barros, G. Shahbazian, and J. P. Cancela, Morphology and morphometry of lycaenid eggs (lepidoptera: Lycaenidae), Zootaxa **3937**, 201 (2015).

[5] E. Katifori, S. Alben, E. Cerda, D. R. Nelson, and J. Dumais, Foldable structures and the natural design of pollen grains, Proc. Natl. Acad. Sci. USA **107**, 7635 (2010).

[6] A. Radja, E. M. Horsley, M. O. Lavrentovich, and A. M. Sweeney, Pollen cell wall patterns form from modulated phases, Cell **176**, 856 (2019).

[7] H. Ting-Beall, D. Needham, and R. Hochmuth, Volume and osmotic properties of human neutrophils, Blood **81**, 2774 (1993).

[8] A. C. Rowat, D. E. Jaalouk, M. Zwerger, W. Ung, I. A. Eydelnant, D. E. Olins, A. L. Olins, H. Herrmann, D. A. Weitz, and J. Lammerding, Nuclear envelope composition determines the ability of neutrophil-type cells to passage through micron-scale constrictions*, J. Biol. Chem. **288**, 8610 (2013).

[9] L. Wang, C. E. Castro, and M. C. Boyce, Growth strain-induced wrinkled membrane morphology of white blood cells, Soft Matter **7**, 11319 (2011).

[10] T. Tallinen, J. Y. Chung, J. S. Biggins, and L. Mahadevan, Gyrification from constrained cortical expansion, Proc. Natl. Acad. Sci. USA **111**, 12667 (2014).

[11] M. J. Razavi, T. Zhang, X. Li, T. Liu, and X. Wang, Role of mechanical factors in cortical folding development, Phys. Rev. E **92**, 032701 (2015).

[12] P. Ciarletta, Buckling Instability in Growing Tumor Spheroids, Phys. Rev. Lett. **110**, 158102 (2013).

[13] T. Tanaka, S.-T. Sun, Y. Hirokawa, S. Katayama, J. Kucera, Y. Hirose, and T. Amiya, Mechanical instability of gels at the phase transition, Nature (London) **325**, 796 (1987).

[14] W. Barros, E. N. de Azevedo, and M. Engelsberg, Surface pattern formation in a swelling gel, Soft Matter **8**, 8511 (2012).

[15] J. Dervaux, Y. Couder, M.-A. Guedeau-Boudeville, and M. Ben Amar, Shape Transition in Artificial Tumors: From Smooth Buckles to Singular Creases, Phys. Rev. Lett. **107**, 018103 (2011).

[16] T. Bertrand, J. Peixinho, S. Mukhopadhyay, and C. W. MacMinn, Dynamics of Swelling and Drying in a Spherical Gel, Phys. Rev. Appl. **6**, 064010 (2016).

[17] C. Li, X. Zhang, and Z. Cao, Triangular and fibonacci number patterns driven by stress on core/shell microstructures, Science **309**, 909 (2005).

[18] G. Cao, X. Chen, C. Li, A. Ji, and Z. Cao, Self-Assembled Triangular and Labyrinth Buckling Patterns of Thin Films on Spherical Substrates, Phys. Rev. Lett. **100**, 036102 (2008).

[19] C. Fogle, A. C. Rowat, A. J. Levine, and J. Rudnick, Shape transitions in soft spheres regulated by elasticity, Phys. Rev. E **88**, 052404 (2013).

[20] D. Breid and A. J. Crosby, Curvature-controlled wrinkle morphologies, Soft Matter **9**, 3624 (2013).

[21] N. Stoop, R. Lagrange, D. Terwagne, P. M. Reis, and J. Dunkel, Curvature-induced symmetry breaking determines elastic surface patterns, Nat. Mater. **14**, 337 (2015).

[22] F. Xu, S. Zhao, C. Lu, and M. Potier-Ferry, Pattern selection in core-shell spheres, J. Mech. Phys. Solids **137**, 103892 (2020).

[23] F. Xu, Y. Huang, S. Zhao, and X.-Q. Feng, Chiral topographic instability in shrinking spheres, Nat. Comput. Sci. **2**, 632 (2022).

[24] See Supplemental Material at http://link.aps.org/supplemental/10.1103/PhysRevE.107.065003 for a MATHEMATICA notebook that performs the calculations described.

[25] S. T. Milner and S. A. Safran, Dynamical fluctuations of droplet microemulsions and vesicles, Phys. Rev. A **36**, 4371 (1987).